Ultrasonics 95 (2019) 45–51

Contents lists available at ScienceDirect

Ultrasonics

journal homepage: www.elsevier.com/locate/ultras

Sound regulation of coupled Helmholtz and Fabry-Pérot resonances in labyrinth cavity structures

Yan Liu[a], Hui Zhang[b,*], Jian Yang[a], Xiang Zhang[a], Shu-yi Zhang[a], Li Fan[a], Gen Gu[a]

[a] Key Laboratory of Modern Acoustics, MOE, School of Physics, Nanjing University, Nanjing 210093, PR China
[b] Jiangsu Key Laboratory for Design and Manufacture of Micro-Nano Biomedical Instruments, School of Mechanical Engineering, Southeast University, Nanjing 211189, PR China

ARTICLE INFO

Keywords:
Sound attenuation
Coupling resonance
Helmholtz resonance
Fabry-Pérot resonance

ABSTRACT

Traditional acoustic regulations in practice are used to have major obstacles in low frequency range, for which absorbers or suppressors have thicknesses that are comparable to their working wavelength. We present an acoustic structure-based "coiling-up space" to achieve outstanding sound regulation of acoustic waves in the extremely low frequency region. The structure is composed of an open waveguide and with a spiral throat tube and a cavity. The acoustic structure excites Helmholtz and Fabry-Pérot resonances in labyrinth cavity structures, coupling of an open waveguide, which produce Fano-like resonances respectively and a broadband low-transmission spectrum in the 120–3100 Hz range. During sound regulation, the existing open waveguide can also maintain natural ventilation through the structure. In addition, the sound transmission properties are shown to be sensitive to the structural parameters, which can be used to provide a tunable sound control method for acoustic devices.

1. Introduction

Acoustic regulation has always been a challenging problem in applications including acoustic attenuation, acoustic shielding, noise control and vibration damping, particularly when the regulating material's thickness is much smaller than the wavelength [1,2]. Recently, considerable effort has been devoted to the design of acoustic absorbers or acoustic attenuators that use locally resonant structures to increase absorption rates and provide superior absorptive characteristics when compared with conventional acoustic absorptive materials, e.g., porous materials [3–5]. However, acoustic attenuation at low frequencies remains challenging when using only Bragg scattering or the local resonance [6–10]. However, regardless of whether Bragg scattering or local resonance is used, acoustic attenuation is constrained within a narrow frequency range. Therefore, novel considerations, including use of acoustic holey structures, acoustic membrane structures and acoustic spiral tubes have been proposed for sound regulation over a broad band in the low frequency range [11–15].

The aim of this work is to propose an ultra-thin composite structure that can regulate broadband sound while allowing free ventilation. In the proposed structure, an open waveguide, a labyrinth cavity (composed of a spiral throat tube and a cavity) were designed to realize coupling of resonances and control of low sound transmission over a broad frequency band.

As shown in Fig. 1(a), the composite structure is composed of two different units, where the labyrinth cavity (the spiral tube and the cavity) form a locally resonant unit and the open waveguide acts as a continuous sound unit. Consequently, the labyrinth cavity structure reduces the proposed device thickness substantially. As can be seen from Fig. 1 (b) and Table 1, the device thickness (i.e., the length of the open waveguide) is only $l = 0.0265$ mm, which is far less than one half of the wavelength at the frequency below 4000 Hz. Therefore, an open waveguide is a continuous system in the frequency range.

More specifically, the labyrinth cavity forms a local Helmholtz-like unit at low frequencies, which thus produces Helmholtz resonance. At higher frequencies, the spiral throat tube length ($l_t \approx \frac{\lambda}{2}$) is about twice the cavity height ($l_c \approx \frac{\lambda}{4}$) and Fabry-Pro resonance can thus be generated. The interaction between the continuous sound field state (generated in the open waveguide) and the resonant vibration (generated in the labyrinth cavity) results in peak-dip Fano-like resonances. Between the two Fano-like resonances, a broadband low-transmission spectrum is formed in the 120–3100 Hz range. The composite structure can therefore excite several discrete resonant states, including the Helmholtz and Fabry-Pérot resonances, which are applicable to regulation of sound transmission over a broad frequency range.

* Corresponding author.
E-mail addresses: seuzhanghui@seu.edu.cn (H. Zhang), zhangsy@nju.edu.cn (S.-y. Zhang).

https://doi.org/10.1016/j.ultras.2019.03.007
Received 29 October 2018; Received in revised form 1 March 2019; Accepted 4 March 2019
Available online 06 March 2019
0041-624X/

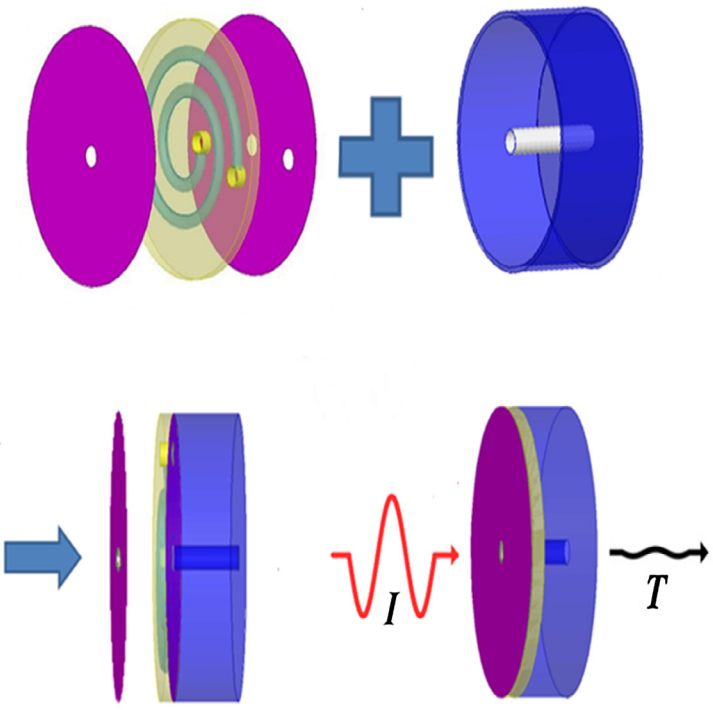

(a)

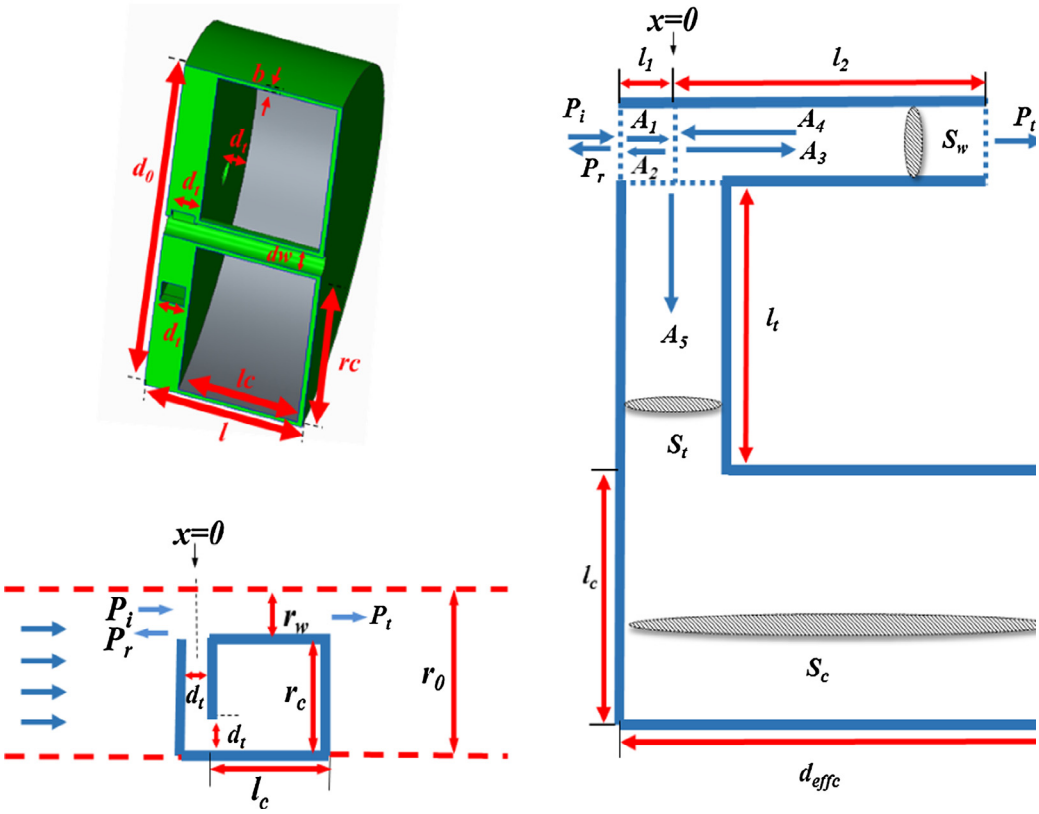

Fig. 1. Schematic diagram of the composite structure. (a) Three-dimensional view. (b) Three-dimensional cross-section view, half axisymmetric 2D cross-sectional view and equivalent 2D cross-section view. The composite structure (height l, wall thickness $b \approx 1.5$ mm, diameter $d_0 \approx 2r_c + d_w + 4b$, radius r_0 and sectional area $S_0 = \frac{\pi d_0^2}{4}$) is composed of two different units. One is the open waveguide (length $l = l_1 + l_2$, diameter d_w, radius r_w, sectional area $S_w = \frac{\pi d_w^2}{4}$) regarded as a continuous sound field unit. The other is a locally resonant unit consist of the spiral tube (length l_t, diameter d_t, radius r_t, and sectional area $S_t = \frac{\pi d_t^2}{4}$) and the circle cavity (cavity height l_c, effective diameter $d_{effc} \approx \sqrt{d_0^2 - d_t^2}$, circle radius r_c and cavity sectional area $S_c \approx \frac{\pi(d_0^2 - d_t^2)}{4}$ when the thin wall thickness is ignored).

Table 1
Background medium properties and structural dimensions used in the simulations.

ρ (Kg/m^3)	c_0 (m/s)	$d_w = 2r_w$ (mm)	$d_w = 2r_w$ (mm)	r_c (mm)	l_t (mm)	l_c (mm)	l_1 (mm)	l_2 (mm)
1.21	344	6	5	34	48	24	1.5	25

2. Methods

2.1. Theoretical model of wave propagation

In the theoretical model, the plane wave is assumed to be radiated on the device. The parameters used in our investigations are listed in Table 1. As shown in Fig. 1(b) the equivalent cross-section view, the spiral throat tube is straightened, connecting the open waveguide the cavity. The device thickness (i.e., the length of the open waveguide) is only $l = l_1 + l_2 = 0.0265$ mm. The spiral throat tube effective length is about twice the cavity height. In the junction position $x = 0$, i.e., the connection between the open waveguide and straightened long tube with cavity, the sound pressures are the same, it can be obtained that

$$A_1 + A_2 = A_3 + A_4 = A_5, \tag{1}$$

The volume velocities of the outflow and the inflow in the junction are equal, which satisfies the relation [8]

$$(A_1 - A_2)/Z_w = (A_3 - A_4)/Z_w + A_5/Z_r, \tag{2}$$

where Z_r represents the effective impedance of the shunt resonator (labyrinth cavity), and Z_w represents the distributed acoustic impedance of open waveguide.

On the other hand, there is the continuity of the sound pressure and volume velocity related to the incident sound field:

$$P_i + P_r = A_1 e^{ikl_1} + A_2 e^{-ikl1} \tag{3}$$

$$(P_i - P_r)/Z_0 = (A_1 e^{ikl_1} - A_2 e^{-ikl_1})/Z_w \tag{4}$$

If a free sound field is considered at the outlet end, there is only transmission wave in the outlet end. Therefore the sound pressure and volume velocity can be given as

$$A_3 e^{-ikl_2} + A_4 e^{ikl_2} = P_t, \tag{5}$$

$$(A_3 e^{-ikl_2} - A_4 e^{ikl_2})/Z_w = P_t/Z_0, \tag{6}$$

where P_i, $P_r$and P_t denote the sound pressure of the incident, reflected and transmitted sound fields, respectively. Z_0 denotes the structure acoustic surface impedance. l_1 and l_2 are the distances from the input and output surfaces to the center of the connection point between the spiral throat tube and the open waveguide.

Thus, the general solution can be written as

$$B[A_1 A_2 A_3 A_4 A_5 P_r P_t]^T = P, \tag{7}$$

where

$$\mathrm{B} = \begin{bmatrix} 1 & 1 & 0 & 0 & -1 & 0 & 0 \\ 0 & 0 & 1 & 1 & -1 & 0 & 0 \\ Z_w{}^{-1} & -Z_w{}^{-1} & -Z_w{}^{-1} & Z_w{}^{-1} & -Z_r{}^{-1} & 0 & 0 \\ e^{ikl_1} & e^{-ikl_1} & 0 & 0 & 0 & -1 & 0 \\ Z_0 Z_w{}^{-1} e^{ikl_1} - Z_0 Z_w{}^{-1} e^{-ikl_1} & 0 & 0 & 0 & 1 & 0 & \\ 0 & 0 & e^{-ikl_2} & e^{ikl_2} & 0 & 0 & -1 \\ 0 & 0 & Z_0 Z_w{}^{-1} e^{-ikl_2} - Z_0 Z_w{}^{-1} e^{ikl_2} & & 0 & 0 & -1 \end{bmatrix},$$

and $P = [0001100]^T P_i$,

2.2. Transmission coefficient and the shunt resonator impedance Z_r

To illustrate the working mechanisms of the proposed composite structure more clearly, we investigate its sound transmission properties from the above matrix. The composite structure's transmission coefficient [16,17] can be given as

$$T_P = |P_t/P_i| = \frac{4}{|E + F|}, \tag{8}$$

where $E = 4\cos(kl) + 2i\sin\left[kl\left(\frac{Z_w}{Z_0} + \frac{Z_0}{Z_w}\right)\right]$

$F = \frac{Z_w}{Z_r}\left\{\cos\left[kl\left(\frac{Z_w}{Z_0} + \frac{Z_0}{Z_w}\right)\right] + 2i\sin(kl) - \cos\left[k\Delta l\left(\frac{Z_w}{Z_0} - \frac{Z_0}{Z_w}\right)\right]\right\}$; k is the wave vector. $l = l_1 + l_2$, $\Delta l = l_2 - l_1$. A detailed depiction of the structure is shown in Fig. 1. The transmission coefficient T_p has a close relationship with the shunt resonator (labyrinth cavity) impedance $Z_r$and the acoustic components impedance Z_β, where the subscripted $\beta = 0, w, t,$ and c denote the surface, the open waveguide, the spiral throat tube and the annular cavity, respectively.

If the viscous friction is considered, the acoustic impedance Z_β can be given by

$$Z_\beta = \frac{\rho c_0}{S_\beta}\left\{1 + \frac{\alpha d_v}{r_\beta}[1 - (\gamma - 1)/\chi]\right\}, \tag{9}$$

where ρ and c_0 are the density of air and the sound velocity in the air, respectively; S_β denotes the cross-sectional area of different parts of the structure; r_β represents the effective radius for each of the different structures; $d_v = \sqrt{2\mu/\rho\omega}$ is the thickness of the viscous boundary layer, where $\mu = 1.568 \times 10^{-5}$ m^2/s is the air viscosity and ω is angular frequency; the Prandtl number $\chi = \sqrt{P_r}$, where $P_r = 0.702$; $\alpha = (1 - i)/\sqrt{2}$; and the heat capacity ratio $\gamma = 1.4$.

Normally, Z_β will not be zero. In particular, if $Z_r = 0$, $T_P = |P_t/P_i| = \frac{4}{|E+F|} = 0$; the transmittance will be zero.

The shunt resonator (labyrinth cavity) impedance Z_r is closely related to its structure and frequency. As shown in Fig. 1(b), the resonator consists of the spiral tube and the cavity. When the cavity bottom is a rigid wall, the impedance at the bottom can be considered as infinite. According to the acoustic impedance transfer formula, the impedance at the cavity open side (That is, the junction between the spiral tube and the cavity.) is $Z_2 = -iZ_c cot(kl_c)$. Then Z_2 is transferred to the spiral tube other opening (That is, the junction between the spiral tube and open waveguide.) to get $Z_r = Z_t\frac{(Z_2/Z_t) + itan(kl_t)}{1 + i(Z_2/Z_t)tan(kl_t)}$. Then, we can find $Z_r = \frac{-iZ_c cot(kl_c) + iZ_t tan(kl_t)}{1 + (Z_c/Z_t)(tan(kl_t)/tan(kl_c))}$. l_c is the cavity height, $l_t$is the spiral tube effective length. Z_t and Z_c are distributed impedance of spiral tube and cavity respectively, which can be calculated from Eq (9). The cross-sectional area of the cavity is much larger than that of the the spiral tube and $Z_c \ll Z_t$ can be deduced.

At low frequencies, the denominator $1 + \frac{Z_c}{Z_t}\left(\frac{tan(kl_t)}{tan(kl_c)}\right) \approx 1 + \frac{Z_c}{Z_t}\left(\frac{kl_t}{kl_c}\right) \approx 1$, Z_r is simplified to $iZ_t tan(kl_t) - iZ_c cot(kl_c)$. As shown in Table 1, l_t and l_c are fixed values and $l_t \approx 2l_c$. At high frequencies, the denominator $1 + \frac{Z_c}{Z_t}\left(\frac{tan(kl_t)}{tan(kl_c)}\right) = 1 + \frac{Z_c}{Z_t}\left(\frac{2}{1 + tan^2(kl_c)}\right)$ and $Z_r = \frac{-iZ_c cot(kl_c) + iZ_t tan(kl_t)}{1 + 1 + \frac{Z_c}{Z_t}\left(\frac{2}{1 + tan^2(kl_c)}\right)}$. The value of $tan^2(kl_c)$ is between 0 and positive infinity. When $tan^2(kl_c) \in [0, +\infty)$, the value of $\frac{2}{1 + tan^2(kl_c)}$ is between 0 and 2, and $Z_c \ll Z_t$, $1 + \frac{Z_c}{Z_t}\frac{2}{1 + tan^2(kl_c)} \approx 1$, then $Z_r \approx iZ_t tan(kl_t) - iZ_c cot(kl_c)$. Therefore, Z_r can be simplified whether in the low frequency range or in the high frequency range.

3. Results

3.1. Fano-like sound transmission profile results at low frequencies

As shown in Fig. 1(b), the connection point is close to the side at which the sound is incident, i.e., $l_2 \gg l_1$, the input impedance of the proposed composite structure can be given approximately as $Z_{in} = \frac{Z_r Z_e}{Z_r + Z_e}$, where $Z_e = iZ_w \tan(kl_2)$ represents the open waveguide acoustic impedance at the connection point. Normally, Z_β will not be zero for l_2 is far less than one half of the wavelength. In this case, when $Z_r \approx iZ_t \tan(kl_t) - iZ_c \cot(kl_c) \approx 0$, $Z_{in} \approx 0$ means that there is impedance mismatch on the incident side of the composite structure. At low frequencies, $tan(kl_t)$ and $cot(kl_c)$ can be simplified to the forms kl_t and $\frac{1}{kl_c}$, respectively. $k = \frac{\omega}{c_0}$ is the wave vector and $\omega = 2\pi f$ is angular frequency. When $Z_r \approx 0$, $Z_t kl_t = \frac{Z_c}{kl_c}$. Consequently, transmission coefficient T_P is close to 0 (a transmission dip) from Eq (8) and $f_{1,d} = \frac{c_0}{2\pi}\sqrt{\frac{S_t}{l_t l_c S_c}}$ is induced when ignoring the viscous friction.

The sound transmission dip can also be explained by the occurrence of a resonant vibration in the labyrinth cavity (the spiral tube and the cavity). In general, the spiral tube and the cavity can be regarded as a Helmholtz cavity in the low frequency regime, where the two components are analogous to an acoustic capacitor (where $C = \frac{V}{\rho c_0^2}$, $V = S_c l_c$) and an acoustic mass ($M = \frac{\rho}{S_t} l_t$), respectively. The resonant frequency of the Helmholtz cavity is given by $f_{1,h} = \frac{c_0}{2\pi}\sqrt{\frac{S_t}{l_t l_c S_c}}$, which is equal to $f_{1,d}$, thus demonstrating that the transmission dip at around 120 Hz can be attributed to the resonant vibration in the cavity and the spiral tube. As shown in Fig. 2(a), there is phase change from negative to positive in the propagating and a transmission dip around the resonant state of this resonant unit.

However, the open waveguide can be always regarded as a continuous unit at low frequencies. When the spiral tube and the cavity form a resonant unit at 120 Hz, the continuous unit is coupled to the resonant unit. As shown in Fig. 2(b), the Fano-like sound transmission profile of composite structure near 120 Hz can then be excited [18–20] in this case, for which sound interference occurs between the resonant unit and the continuous unit. On the other hand, the open waveguide (continuous unit) length is much smaller than the wavelength at low frequencies, so the Fano-like sound transmission profile can be freely tuned via adjustment of resonant unit (he spiral tube and the cavity) structural parameters.

3.2. Fano-like asymmetric profile results at high frequencies and impedance analysis

It has previously been proven that a single Helmholtz resonator (HR) can form a narrow-band notch filter to restrain sound. To achieve broadband sound reduction, new modes must be excited to broaden the resonator's bandwidth via multi-mode coupling.

At higher frequencies, when $\tan(kl_t)$and $\cot(kl_c)$ are zeros respectively, the shunt resonator impedance $Z_r \approx iZ_t \tan(kl_t) - iZ_c \cot(kl_c)$ is 0 and transmission coefficient T_P is close to 0. The term of $tan(kl_t) = 0$ yields to $kl_t = n\pi$, $l_t = n\lambda/2 (n = 0, 1, 2, 3\cdots)$, where $\lambda = \frac{2\pi f}{c_0}$ is the wavelength. The term of $cot(kl_c) = 0$ yields to $kl_c = (2m + 1)\pi/2, l_c = (2m + 1)\lambda/4 (m = 0, 1, 2, 3\cdots)$. Considering the actual processing and manufacturing, $l_t = 2l_c = \lambda/2 (n = 1, m = 0)$. At this case, the shunt resonator impedance is further simplified to $Z_r \approx iZ_t tan(kl_t)$ and the spiral tube in the composite structure can be approximately assumed to be connected to both free sound fields. Thus, if $Z_r \approx 0$, the spiral tube forms a resonant unit with resonance frequencies of $f_{2,d} = nc_0/2l_t (n = 1, 2, 3\cdots)$ ideally, which are equal to the frequencies of Fabry-Pérot resonance [21]. In this case, the spiral throat tube effective length ($l_t \approx \frac{\lambda}{2}$) is about twice the cavity effective height ($l_c \approx \frac{\lambda}{4}$) and Fabry-Pérot resonance is excited in the spiral throat tube. As shown in Fig. 2(c), the resonant unit has a transmission peak (which has a symmetric Lorentzian profile) and a phase change at the Fabry-Pérot resonance at approximately 3300 Hz considering the viscous friction.

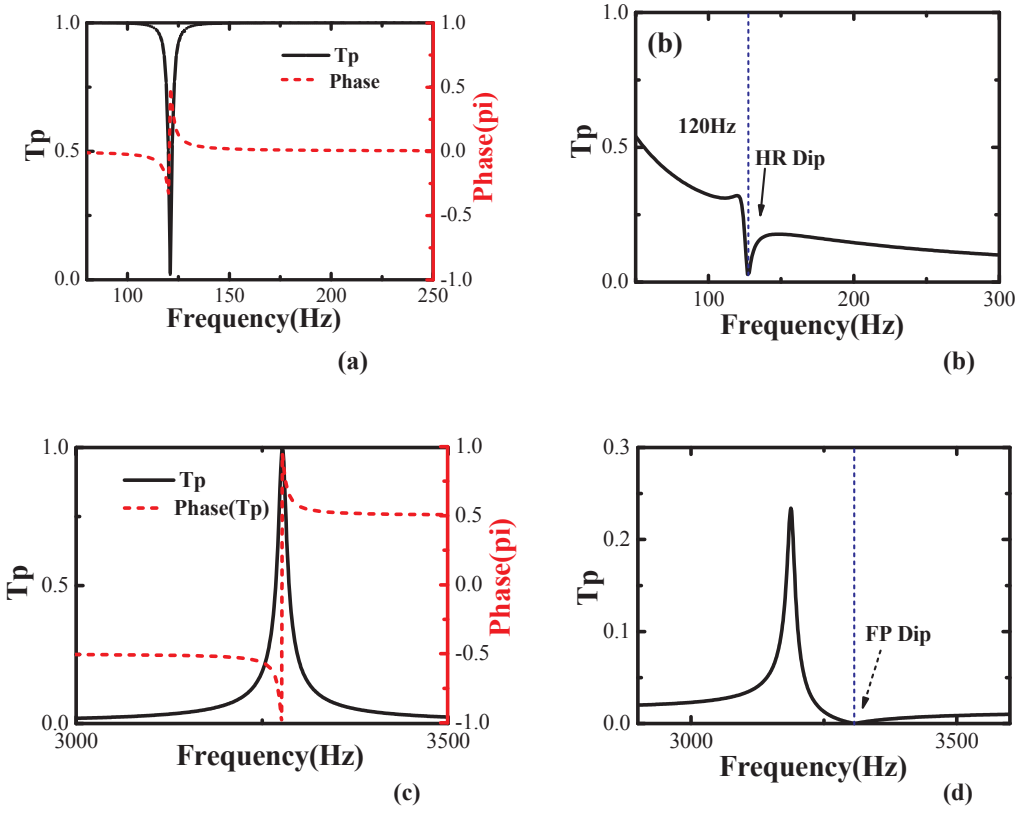

Fig. 2. Transmission spectra of the resonant unit, its phase change, and the Fano-like sound transmission profile (the resonant unit is coupled to the continuous unit) versus low or high frequency. (a) Transmission dip of the resonant unit (the shunt Helmholtz-like resonator) and its phase change around 120 Hz. (b) The Fano-like sound transmission profile of the composite structure around 120 Hz. (c) Transmission peak of the resonant unit (the spiral tube) and its phase change around 3300 Hz. (d) The Fano-like sound transmission profile of the composite structure around 3300 Hz.

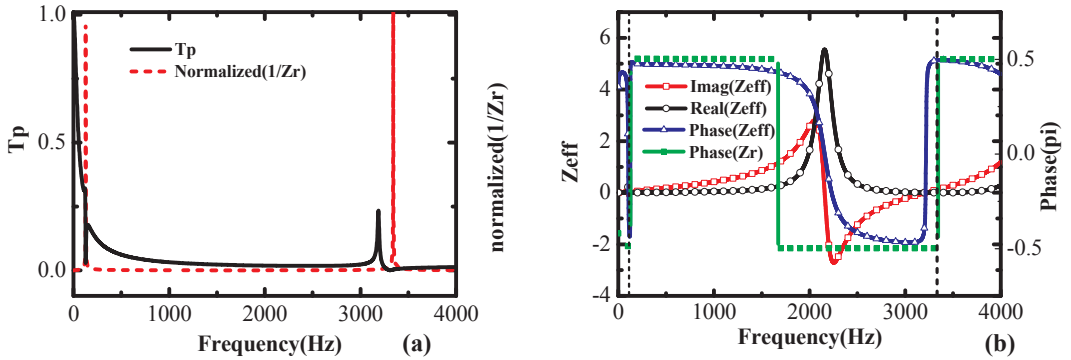

Fig. 3. (a) Transmission spectrum below 4000 Hz for the composite structure and the reciprocal of the resonant unit impedance Z_r. (b) The real part, the imaginary part and the phase of Z_{eff} and the phase of the locally resonant unit Z_r.

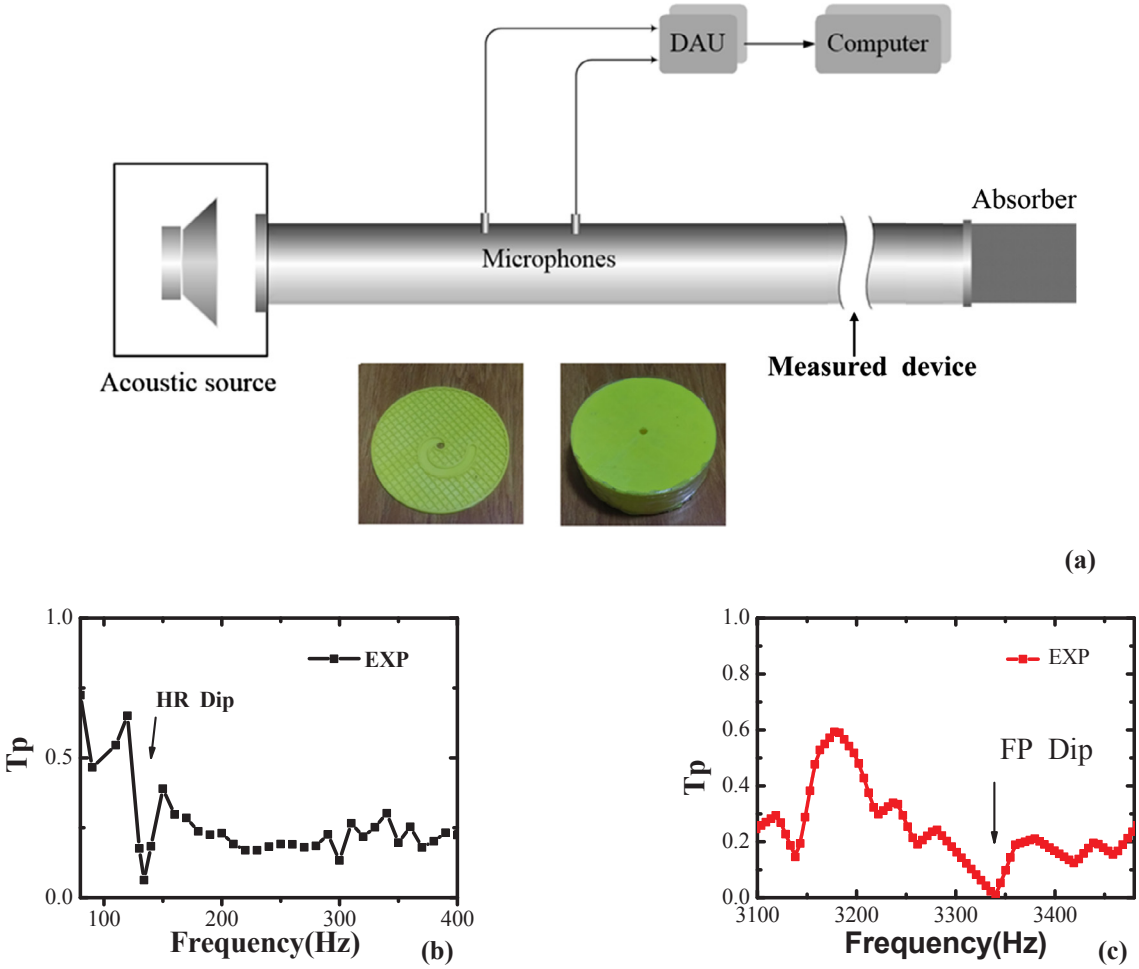

Fig. 4. (a) Experimental setup used to measure the transmission spectrum of the composite structure. (b) and (c) show the transmission spectra around 120 Hz and 3300 Hz, where the downward arrows indicate the frequencies of the Helmholtz dip and the Fabry-Pérot dip, respectively.

However, the open waveguide length is still less than one half of the wavelength, i.e., there is no standing wave resonance in it, and the open waveguide is still a continuous unit. Consequently, the Fabry-Pérot resonant states in the spiral tube can be coupled to the continuous states in the open waveguide, which results in a Fano-like asymmetric transmission curve profile (peak around 3200 Hz, dip around 3350 Hz), as shown in Fig. 2(d). At the transmission peak of the Fano-like sound transmission profile, the composite structure produces destructive interference near the input side, which then guides more of the acoustic energy into the output side. At the transmission dip, the composite structure produces enhanced interference near the input side; as a result, most of the acoustic energy is reflected and very little acoustic energy can then be transmitted to the output side.

To provide further confirmation of the above analysis, the transmission curve and the reciprocal resonator impedance $1/Z_r$ are investigated. Fig. 3(a) shows that $1/Z_r$ has a value that is close to infinity at the transmission dips (T_P are close to 0), indicating that resonances occur and thus further verifying the analysis results. In addition, the resonator impedance phases are investigated, are shown in Fig. 3(b). The first black vertical dashed line (around 120 Hz) represents Helmholtz resonance frequency, and the second black vertical dashed line (around 3350 Hz) represents Fabry-Pérot resonance dip. As can be seen

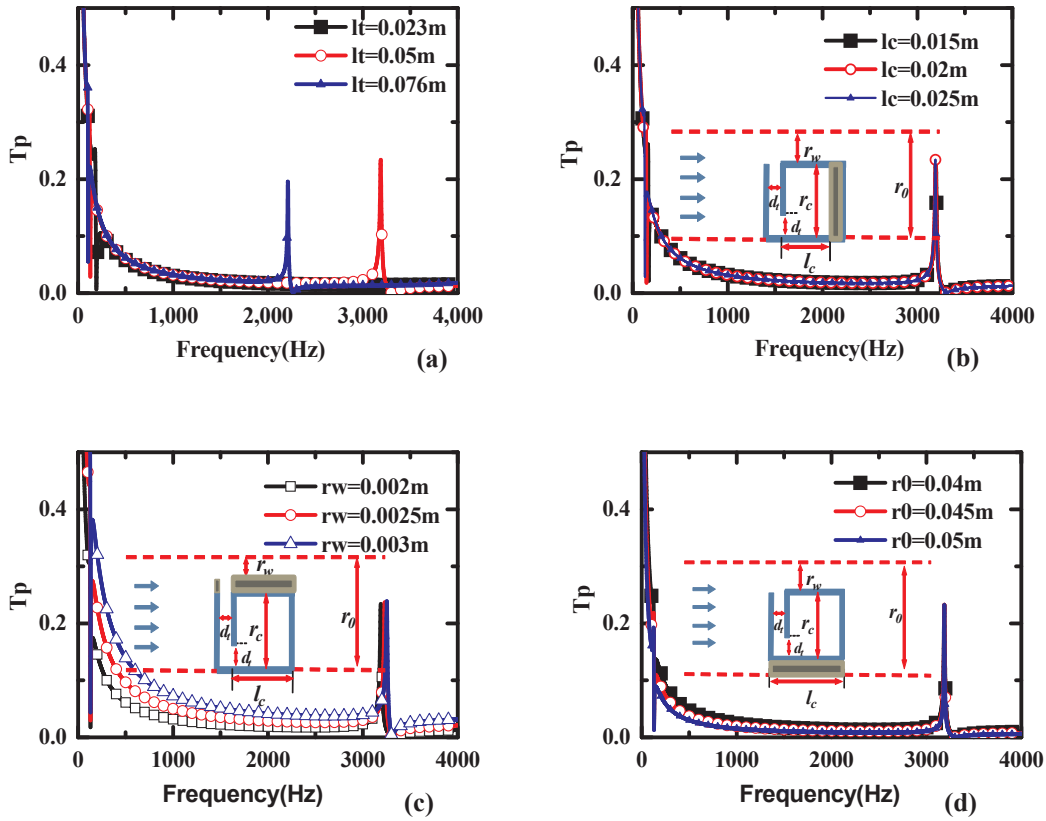

Fig. 5. Transmission spectra below 4000 Hz for various spiral tube length (l_t), various cavity height (l_c), various open waveguide radius (r_w) and various composite structure radius (r_0). The insets in Fig. 5(b)–(d) are half of the axisymmetric two-dimensional cross-section, showing how to change the parameters. The spiral tube length (l_t) can be increased or shortened directly for the spiral tube is coplanar and other parameters remain unchanged. The inset in Fig. 5(b) shows the cavity height (l_c) can be reduced by increasing the thickness of the cavity bottom inner side and other parameters of the device remain unchanged. The inset in Fig. 5(c) shows the waveguide inner radius (r_w) can be reduced by increasing the waveguide inner wall thickness and other parameters of the device remain unchanged. The inset in Fig. 5(d) shows the composite device radius (r_0) is increased by increasing the device outer wall thickness, while other parameters remain unchanged.

from Fig. 3(a) and (b), at these two frequency positions, the local resonant unit impedance $Z_r \approx 0$ and the phase of the local resonant unit (Z_r) reverses from negative to positive and as a result the sound transmission dips are to be generated.

In addition, the relationship between the normalized input impedance and its phases is investigated. The normalized input acoustic impedance on the input side is $Z_{eff} = \frac{Z_{in}}{Z_w}$, in which Z_w can be calculated from Eq (9). As shown in Fig. 3(b), between two discrete Fano-like resonances, the acoustic resistance (i.e., Real(Z_{eff})) radiates the energy out and the acoustic reactance (i.e., Imag(Z_{eff})) reflects the energy back. When the phase of the normalized input acoustic impedance (i.e., ($phase(Zeff)$)) is not zero, the acoustic energy oscillates in the device, and the transmittance is low. When the frequency is about 2200 Hz and the phase(Z_{eff}) = 0, it means that Z_{eff} is the pure acoustic resistance excluding the acoustic reactance. However, the acoustic resistance also reaches its maximum and transmission is low.

When the frequency is a little below 120 Hz or a little below 3300 Hz (round 3200 Hz), the phase of the normalized input acoustic impedance ((phase(Zeff)) goes from negative to positive. This means that the system shifts from vibrating out-of-phase to in-phase with respect to the external harmonic excitation. We also found the Fano-like asymmetric transmission peak is below resonance and the phase difference of Z_{eff} and Z_r is close to π in Fig. 3(b). This phenomenon is in agreement with the interference of both resonant and non-resonant paths. It can be seen in Ref. [22] for more details. However, the impedance Z_{eff} phase goes from negative to positive, involved in the coupling of resonances, which means that impedance matching occurs around the resonances and the sound transmission peaks are thus generated. Simultaneously, severe impedance mismatching occurs on the input side over the range from 120 Hz to 3100 Hz and a broadband low-frequency sound transmission occurs.

4. Experiments and discussions

The experimental measurements were carried out as shown in Fig. 4(a). The measurement samples were fabricated from epoxy resin using 3D-printing technology. A loudspeaker was used to excite the acoustic waves in the main waveguide, and two tiny microphones were set up to detect the acoustic pressure in front of the sample. The received signals were then input into a computer via a data acquisition unit (DAU) for subsequent processing. Fig. 4(b) and (c) show the sound pressure transmission characteristics at normal incidence near frequencies of 120 Hz and 3200 Hz, respectively. The sound transmission characteristics show the dips that indicate the weakening of the transmitted waves.

We have investigated the effects of structural parameters on sound transmission to understand how sound transmission can be regulated over a wide frequency range.

As shown in Fig. 5(a)–(b), the effects of l_t and l_c on the transmission spectra produce different tendencies. For example, l_t or l_c can influence the first dip and l_t can change the Fano-like asymmetric transmission profile obviously in the high frequency range. When l_t is shortened, the Helmholtz resonance frequency decreases slightly; however, for Fabry-Pérot resonance, it means that one half of the wavelength decreases greatly and the frequency decreases significantly. When l_c is decreased, the Helmholtz resonance frequency decreases slightly and the Fabry-Pérot resonance frequency basically remains unchanged. This result shows that when the cavity height (l_c) varies in a limited range, it has

little effect on the Fabry-Pérot resonance frequency, coinciding with the previous numerical analysis. We can thus adjust l_t to change the Fabry-Pérot resonance in the high frequency range to regulate the bandwidth of low transmission spectrum.

However, the attenuation of broadband low-frequency acoustic transmission increases with the decrease of waveguide radius (r_w), as shown in Fig. 5(c). When r_w decreases, the resonance frequency remains unchanged and the ventilation rate will inevitably decrease. The transmittance decreases for the friction.

In addition, Fig. 5(d) shows that as the radius (r_0) of the device increases, the sound transmittance then decreases. The increase of the device radius (r_0) means that the device cross-section becomes larger. Obviously, the equivalent incident impedance increases and the transmittance decreases, but the resonance states remain unchanged.

This indicates that the transmission characteristics are sensitive to the structural parameters, and the sound transmission can be adjusted by adjusting the structural parameters. In addition, noise insulation with a wide low frequency range and ventilation can be achieved by coupling of the resonances between the continuous sound unit and the resonant sound unit.

5. Conclusions

In summary, we report a composite acoustic structure that can be used to regulate sound transmission. This structure has a sub-wavelength thickness that is capable of blocking a broad frequency range while also providing a high ventilation capability. These extraordinary features are produced by coupling effects between the multimode resonant states in the resonant sound unit and the continuous states in the continuous sound unit. The transmission spectrum can be controlled by adjusting the structural parameters, which offers potential for regulation of sound transmission over a much wider frequency range.

Acknowledgments

The authors acknowledge the financial support provided by the National Natural Science Foundation of China (Grant Nos. 11874110 and 11774169), and the Special Fund for Research in Quality Inspection of Public Welfare Industry (Grant No. 201510068), and were also sponsored by NUPTSF (Grant No. NY215166).

Appendix A. Supplementary material

Supplementary data to this article can be found online at https://doi.org/10.1016/j.ultras.2019.03.007.

References

[1] D. Zhao, Transmission loss analysis of a parallel-coupled Helmholtz resonator network, AIAA J. 50 (2012) 1339–1346.
[2] J.B. Li, Y.S. Wang, C. Zhang, Tuning of acoustic bandgaps in phononic crystals with Helmholtz resonators, J. Vib. Acoust. 135 (2013) 031015.
[3] C. Zhang, X. Hu, Three-dimensional single-port labyrinthine acoustic metamaterial: perfect absorption with large bandwidth and tunability, Phys. Rev. Appl. 6 (2016) 064025.
[4] V. Romero-Garcia, G. Theocharis, O. Richoux, A. Merkel, V. Tournat, V. Pagneux, Perfect and broadband acoustic absorption by critically coupled sub-wavelength resonators, Sci. Rep. 6 (2016) 19519.
[5] Y.S. Choy, L. Huang, C. Wang, Sound propagation in and low frequency noise absorption by helium-filled porous material, J. Acoust. Soc. Am. 126 (2009) 3008–3019.
[6] Z. Chen, L. Fan, S. Zhang, H. Zhang, X. Li, J. Ding, An open-structure sound insulator against low-frequency and wide-band acoustic waves, Appl. Phys. Exp. 8 (2015) 107301.
[7] Z. Tao, W. He, Y. Xiao, W. Zhang, X. Wang, Sound transmission within the Bragg gap via the high-order modes in a waveguide with periodically corrugated walls, J. Appl. Phys. 105 (2009) 145.
[8] M.T. Islam, G. Newaz, Metamaterial with mass-stem array in acoustic cavity, Appl. Phys. Lett. 100 (2012) 509.
[9] A. Khelif, A. Choujaa, S. Benchabane, B. Djafari-Rouhani, V. Laude, Guiding and bending of acoustic waves in highly confined phononic crystal waveguides, Appl. Phys. Lett. 84 (2004) 4400–4402.
[10] C. Shen, Y. Jing, Side branch-based acoustic metamaterials with a broad-band negative bulk modulus, Appl. Phys. A 117 (2014) 1885–1891.
[11] G. Ma, M. Yang, S. Xiao, Z. Yang, P. Sheng, Acoustic metasurface with hybrid resonances, Nat. Mater. 13 (2014) 873–878.
[12] Y. Xie, B.I. Popa, L. Zigoneanu, S.A. Cummer, Measurement of a broadband negative index with space-coiling acoustic metamaterials, Phys Rev. Lett. 110 (2012) 175501.
[13] Y. Li, B.M. Assouar, Acoustic metasurface-based perfect absorber with deep sub-wavelength thickness, Appl. Phys. Lett. 108 (2016) 204301.
[14] X. Cai, Q. Guo, G. Hu, J. Yang, Ultrathin low-frequency sound absorbing panels based on coplanar spiral tubes or coplanar Helmholtz resonators, Appl. Phys. Lett. 105 (2014) 121901–121901-4.
[15] X. Zhu, K. Li, P. Zhang, J. Zhu, J. Zhang, C. Tian, Implementation of dispersion-free slow acoustic wave propagation and phase engineering with helical-structured metamaterials, Nat. Comm. 7 (2016) 11731.
[16] N. Nemati, A. Kumar, D. Lafarge, N.X. Fang, Nonlocal description of sound propagation through an array of Helmholtz resonators, Comptes rendus – Mécanique 343 (2015) 656–669.
[17] H. Zhang, Z. Wei, L. Fan, J. Qu, S. Zhang, Tunable sound transmission at an impedance-mismatched fluidic interface assisted by a composite waveguide, Sci. Rep. 6 (2016) 34688.
[18] C. Goffaux, J. Sanchez-Dehesa, A. Levy Yeyati, Ph. Lambin, A. Khelif, J.O. Vasseur, B. Djafari-Rouhani, Evidence of fano-like interference phenomena in locally resonant materials, Phys. Rev. Lett. 88 (2002) 225502.
[19] C. Genet, M.P. van Exter, J.P. Woerdman, Fano-type interpretation of red shifts and red tails in hole array transmission spectra, Opt. Commun. 225 (2003) 331–336.
[20] Y.S. Joe, A.M. Satanin, C.S. Kim, Classical analogy of Fano resonances, Phys. Scri. 7463 (2006) 259–266.
[21] H. Zhang, L. Fan, J. Qu, S. Zhang, Sound transmission properties assisted by the phase resonances of composite acoustic gratings, J. Appl. Phys. 119 (8) (2016) 084902.
[22] N. Fang, D. Xi, J. Xu, M. Ambati, W. Srituravanich, C. Sun, X. zhang, Ultrasonic metamaterials with negative modulus, Nat. Metam. 5 (6) (2006) 452–456.